Mechanical behaviour of FRP beam-to-column bolted connections

João Duarte Rocha Serra Mendes

Department of Civil Engineering, Architecture and Georesources, Instituto Superior Técnico, Universidade de Lisboa

Abstract: This dissertation presents an experimental and numerical study about the behaviour of bolted connections between GFRP pultruded profiles and stainless steel angles. In the experimental campaign the mechanical properties of GFRP and stainless steel were measured. Seven types of double-lap connections were tested with GFRP and stainless steel specimens, where the edge distance, the number of bolts and the thickness of the specimen were varied. Four types of beam-to-column connections were loaded monotonically, using stainless steel cleats: one was web-cleated and the other three were flange-cleated. The thickness of the cleats was varied as well as the number of bolts. In both double-lap and beam-to-column tests the connections' resistance, stiffness and ductility were determined. All the connections tested were numerically modelled using Abaqus with Hashin's damage criterion and a progressive damage model based on the fracture energies of GFRP. Overall, the beam-to-column connections tested presented relatively low stiffness and resistance; the strength was very much limited by the lack of continuity of the reinforcing mats between the web and the flanges of the GFRP profile. In addition, no significant increment of strength was found in the typologies with more bolts. Moreover, the cleats' thickness was found to be fundamental to the connection's performance. In fact, the connections with 8 mm thick cleats resisted to higher loads and were stiffer than the connections with 3 mm thick cleats. The numerical models developed presented some limitations, mostly in determining the connections' stiffness. As for the fracture energies of GFRP, it was found that their correct definition has a significant influence in the accurate modelling of the behaviour of the connections.

Keywords: Pultruded GFRP profiles; Lap connections; Beam-to-column connections; Stainless steel cleats; Experimental tests; Numerical Analysis.

1. Introduction

Fiber reinforced polymer (FRP) composites are made of a fibre reinforcement and a polymeric matrix. The types of fibre reinforcements normally used are glass, carbon or aramid, which are impregnated by the matrix. The most commonly used FRPs in the construction industry are glass FRPs (GFRP) due to (i) high resistance-to-weigth ratio; (ii) low self-weight; (iii) high durability even in aggressive environments; and (iv) low maintenance costs. On the other hand, GFRP has a relatively low elasticity modulus and brittle failure.

Among all the producing methods, pultrusion is the most used, since it presents lower production costs. Pultrusion manufacturing results in constant cross-section FRP profiles with much higher properties in the longitudinal direction and orthotropic behaviour, with unique failure modes.

Deformability is a governing factor in the design of GFRP members, as well as the design of connections, which often sets the geometry of the cross-section to be used.

Initially, the geometry of the connections was copied from steel structures. GFRP angles were used to connect the web of the beam to the flange of the column and the connection was designed as nominally pinned. This led to very large deformations and inefficient profile selections.

Various systems were developed to increase the stiffness of connections, allowing their design as semi-rigid. These systems comprised GFRP angles in the flanges. Despite the better results, they were not satisfactory yet. For that reason, other connection elements were developed. However, their results were also considered not satisfactory.

I-section profiles are the most used due to their resemblance to steel structures and their ease of production. Nevertheless, they are susceptible to buckling and one of their unique failure modes is through the web-flange junction.

Ductility is also a matter of concern to designers of GFRP structures, since the material does not guarantee any capacity to dissipate energy. This study is motivated by the need to develop connection systems capable of increasing not only the ductility of connections, but also their stiffness and resistance. To seek this, stainless steel angles were used.

The behaviour of the connections was studied with experimental tests and numerical modelling. The understanding of the material behaviour was crucial to ensure a good design approach and to simulate properly the numerical models.

Characterization tests were performed in GFRP specimens subjected to different load conditions to evaluate their mechanical response. Double-lap experiments were carried out in five types of connections between GFRP specimens, where the edge distance and the number of bolts were varied. Two types of connections with stainless steel specimens were also tested, with varying plate thickness. The last step of the experimental program was the study of four types of full-scale beam-to-column bolted connections subjected to a monotonic loading. The connections' resistance, stiffness and ductility were evaluated and determined. All the connection types (double-lap and beam-to-column) were modelled using Abaqus.

2. Literature review

A connection between GFRP elements can be (i) bolted; (ii) bonded; or (iii) hybrid (bolted and bonded). Bonded connections provide more uniform stress transfer among the FRP elements but raises durability concerns. Bolted connections were initially copied from steel structures and accommodate stress concentrations around the bolts' holes. The advantage of hybrid connections is redundancy, since the bolts are just a safety precaution (backup) and loads are resisted by the adhesive [1].

To study the failure modes of the connection and its behaviour before failure, single-lap and double-lap tests were conducted by several authors (*e.g.* [2–5]). They concluded that the geometry of the connection is the main factor that influences its failure mode. The principal failure modes of a bolted connection are presented in Figure 1.

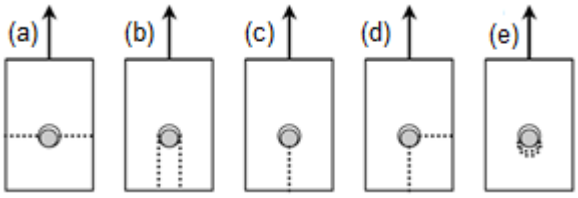

Figure 1 - FRP bolted connections failure modes, adapted from [6]. (a) net-tension; (b) shear out; (c) splitting; (d) cleavage; (e) bearing.

Xiao and Ishikawa [7, 8] studied the bearing failure mode, concluding that this is the only one that can assure failure ductility. Ascione *et al.* [9] studied the influence of the fiber-to-load inclination angle in the bearing failure load. The authors found out that for inclination angles smaller than 10º the influence is much bigger than for bigger angles (0º-90º). In-plane connections were tested varying the number of bolts and the number of rows/columns of bolts [3, 10–12] showing that it is not possible for a multi-bolted connection to fail in bearing. These studies allowed the development of geometric pre-design rules [6, 13, 15] which consider the stress distribution between the different bolts or rows/columns.

The first experimental campaigns developed to study beam-to-column connections [16, 17] tested different types of GFRP cleat angles. The connections' strength and stiffness were considered not suitable which motivated Mosallam *et al.* [18] and Bank *et al.* [19] to develop improved GFRP angles, illustrated in Figure 2, capable of improving the performance of the connection.

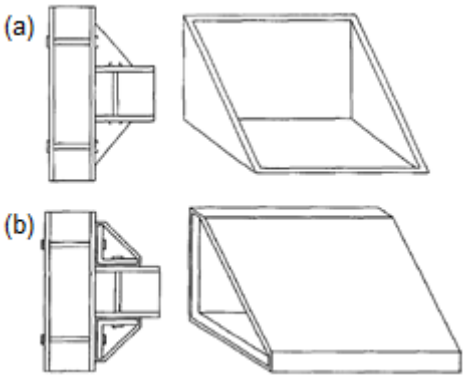

Figure 2 – (a) Mosallam *et al.* [18]; (b) Bank *et al*. [19]. Adapted from [20].

Smith *et al.* [20] compared these two solutions concluding that the one presented in Figure 2 (b) assures more resistance, stiffness and it is easier to produce and assemble.

Qureshi and Mottram [21–24] studied steel and GFRP web-cleated connections. Steel cleats doubled the stiffness provided by GFRP cleats. However, the failure mode of these connections occurred in the web-flange junction, emphasizing the GFRP unique failure modes.

Most numerical studies regarding GFRP connections require the definition of a damage initiation criterion (Tsai-Wu, Tsai-Hill and Hashin are the most commonly used). These criteria only characterise the connection's behaviour until the failure initiation; damage evolution is simulated using damage progression models, which can be constant or continuous, the former being too conservative [25].

In-plane or beam-to-column connections can be modelled. McCarthy and his research team studied single and double-lap connections, single and multi-bolted [26]. In their studies, the authors studied the effects of friction [27] and gaps [28, 29]. Hashin's damage criterion was used and symmetry simplifications were made.

Casalegno *et al.* [30] and Casalegno and Russo [31] used three damage initiation models and a constant degradation model to simulate the connections tested by Bank *et al.* [16]. The strength, stiffness and failure modes were similar to the experimental ones, demonstrating the capacity to predict the behaviour of a bolted connection.

Regardless of these results, as mentioned before, using a continuous progression damage model may have advantages. As such, although the definition of the fracture energies of pultruded GFRP is fundamental, they are still largely unknown.

3. Experimental study

3.1. Experimental program

Coupon tests were performed on specimens extracted from an I cross-section profile (150x75x8x8 mm). The small-scale specimens comprised the following tests: (i) compression; (ii) tension; (iii) flexural; (iv) interlaminar shear; and (v) in-plane shear (Iosipescu shear test) in the longitudinal direction relative to the pultrusion axis. Compression and both shear tests were also conducted in the transverse direction. Stainless steel specimens were subjected to tension tests. These tests aimed at determining the resistance properties of the materials, as well as the elastic moduli.

Double-lap tests were performed in both GFRP and stainless steel coupons, varying the number of bolts and the edge distance.

In addition, four full-scale typologies of beam-to-column connections were tested to determine the resistance, stiffness and (if possible) the ductility of the connections. Two monotonic tests were performed per type of connection.

3.2. Material characterization tests

152 GFRP coupons taken from the web, flanges and a 40 mm wide plate were tested. The average results are presented in Table 1, where the subscripts c, t, f, ci, cp, u, L and T stand for compression, tension, flexural, interlaminar shear, in-plane shear, ultimate value, longitudinal and transverse directions, respectively. Stainless steel specimens 3 mm and 8 mm thick were tested in tension, and the corresponding average results are listed in Table 2 where the subscript y stands for yielding.

GFRP presented an orthotropic behaviour, with higher strength and elastic properties in the longitudinal axis of the profile (the pultrusion direction). In addition, there were also differences between the properties in the web, flange and plate. However, these differences are not significant. In general, the results obtained are in the range of values defined by Gonilha [32]. Nevertheless, the compression and interlaminar shear properties were below that range. On the other hand, the in-plane shear strength exceeded the maximum value expected by 50%.

Poisson's ratio could not be properly determined in stainless steel due to the lack of precision of the video-extensometer used. This lack of precision also affected the determination of the elasticity modulus of the 3 mm thick specimens.

Some specimens' results were not considered due to invalid failure modes or to loss of data during the test.

Table 1 – Average GFRP mechanical properties.

Test Method	Property	Web	Flange	40 mm plate
ASTM D695-02	$\sigma_{cu,L}\ (MPa)$	375	328	318
	$E_{c,L}\ (GPa)$	26,4	22,9	24,6
	$\sigma_{cu,T}\ (MPa)$	42,3	46,7	53,3
	$E_{c,T}\ (GPa)$	2,65	3,91	3,68
EN ISO 527	$\sigma_{tu,L}\ (MPa)$	384	347	367
	$E_{t,L}\ (GPa)$	43,6	41,3	32,1
	$\nu_{LT}\ (-)$	0,22	0,29	0,28
EN ISO 14125	$\sigma_{fu,L}\ (MPa)$	462	393	-
	$E_{f,L}\ (GPa)$	37,0	34,4	-
ASTM D2344	$\sigma_{ciu,L}\ (MPa)$	27,0	29,6	32,4
	$\sigma_{ciu,T}\ (MPa)$	7,41	5,29	-
ASTM D5379-05	$\tau_{cpu,L}(MPa)$	47,7	47,1	52,1
	$G_{LT}\ (MPa)$	3,12	3,14	2,65
	$\tau_{cpu,T}(MPa)$	30,5	27,1	-
	$G_{TL}\ (MPa)$	4,36	2,40	-

Table 2 – Average stainless steel properties in tension.

Test Method	Property	3 mm plate	8 mm plate
EN 1002-1	$\sigma_{tu}\ (MPa)$	651	691
	$\sigma_{ty}\ (MPa)$	363	363
	$E_t\ (GPa)$	-	194
	$\nu\ (-)$	-	-

3.3. Double-lap tests

Four batches of GFRP specimens (DL-15, DL-25, DL-35 and DL-70) were tested, varying the edge distance (15 mm, 25 mm, 35 mm and 70 mm, respectively). The edge distances were determined based on expressions for bearing and shear-out failure modes, according to [6, 14, 33]. It was intended that one of the batches failed by bearing and another one by shear-out. The other two were supposed to be in the transition between these two modes. One batch was tested with two bolts (DL-2P) separated by 35 mm, where the first bolt was centred with an edge distance of 35 mm. Two batches of stainless steel specimens (AISI 304) were also tested, with different specimens' thickness: 3 mm and 8 mm. A2-70 stainless steel bolts were used with a diameter of

8 mm. Four specimens were tested per batch. Figure *3* illustrates a specimen of each batch.

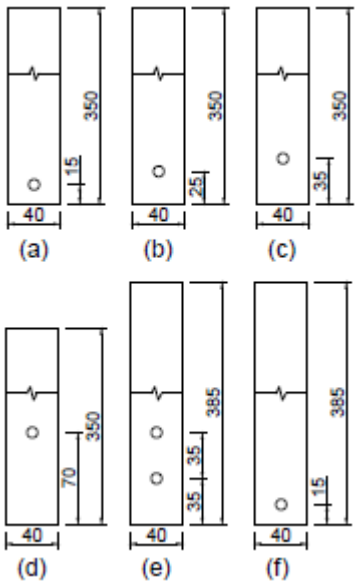

Figure 3 - Double-lap specimens' geometry.

3.3.1.Setup, instrumentation and procedure

The double-lap tests aimed at determining the strength, stiffness and the failure mode of the specimens. A displacement transducer was used to measure the relative displacement between two sections initially separated by 385 mm. The GFRP specimens' strength was considered in the expressions (1) and (2) [14] for shear-out and bearing failure modes, respectively, where (i) V_{so} and $V_{bearing}$ are the design value of strength for shear-out and bearing failure modes, respectively; (ii) $f_{V,Rd}$ and $f_{LR,Rd}$ are the design values of shear and bearing resistance, respectively; and (iii) d, e' and t are the hole diameter, the edge distance and the thickness of the specimen As for the stainless steel specimens, the expressions (3) and (4) [34] were used to determine the specimens' bearing resistance. In this expression (i) $F_{b,Rd}$ is the bearing resistance; (ii) k_1 and α_d are geometric parameters; and (iii) $f_{u,red}$, f_{sy} and f_u are the reduced ultimate, yielding and failure stress in tension of the plate. The bolt shear resistance is given by (5) [34], where (i) V_{bolt} is the bolt shear resistance; (ii) A_f is the shank area of the bolt; and (iii) f_{ub} is the ultimate tensile strength of the bolt.

$$V_{so} = f_{V,Rd} \times (2e' - d) \times t \quad (1)$$

$$V_{bearing} = f_{LR,Rd} \times d \times t \quad (2)$$

$$F_{b,Rd} = k_1 \times \alpha_d \times f_{u,red} \times d \times t \quad (3)$$

$$f_{u,red} = 0{,}5 f_{sy} + 0{,}6 f_u \leq f_u \quad (4)$$

$$V_{bolt} = 0{,}6 \times A_f \times f_{ub} \quad (5)$$

The tests were conducted at a speed of 2 mm/min using a test machine (*INSTRON*, model 1343 with a maximum load capacity of 250 kN).

3.3.2.Results and discussion

The average results for the double-lap tests are presented in Tables 3 and 4, as well as a safety verification for GFRP, stainless steel and bolt.

Table 3 - Average results for double-lap tests with GFRP specimens.

Type	F_u (kN)	δ_u (mm)	K (kN/m)	V_{so} (kN)	$V_{bearing}$ (kN)
DL-15	5,25	0,66	14229	5,24	17,15
DL-25	10,9	0,75	16370	10,1	17,29
DL-35	12,3	0,89	20011	14,9	17,25
DL-70	16,8	18,22	17999	31,6	17,21
DL-2P	19,3	1,83	19690	25,4	29,6

Table 4 - Average results for double-lap tests with stainless steel specimens.

Type	F_u (kN)	δ_u (mm)	K (kN/m)	$F_{b,Rd}$ (kN)	V_{bolt} (kN)
DL-A3	34,4	18,69	23397	22,3	42,2
DL-A8	43,9	6,39	30086	59,6	

The expected shear-out strength for batches DL-15 and DL-25 was considerably close to the experimental strength. The bearing strength for batch DL-70 was also well predicted. As for the batch DL-35, the experimental strength was lower for both failure modes. The proximity of the theoretical strengths suggests a transition of failure mode. Shear-out and bearing failure modes are illustrated in Figure 4.

According to [14], in a metal-GFRP connection with two bolts, the exterior one absorbs 58% of the total load (11,3 kN), which is close to the shear-out strength for the batch DL-35. Despite this, DL-2P was the batch with the greater strength, followed by the batch DL-70. However, the difference in strength (and stiffness) was insignificant. Though, the ultimate displacement was 10 times higher in connection DL-70. The stiffness increased with the increase of the edge distance, with exception of batch DL-70, allowing to conclude that it only increases until a certain plateau, after which it remains approximately constant.

The stiffness of the batch DL-A8 was 34% bigger than that of the batch DL-A3. The bolt's shear resistance was similar to the strength of the batch DL-A8, corresponding to its failure mode. The strength of the batch DL-A3 was between the bolt's shear strength and the plate's bearing resistance. This was possibly due to the large displacements, which led to introducing bending moment in the bolt.

As expected, the stainless steel specimens' performance was better than that of GFRP specimens. This points out the potential advantages of a beam-to-column connection using stainless steel cleats.

Figure 5 presents an experimental force-displacement curve (E) for each batch.

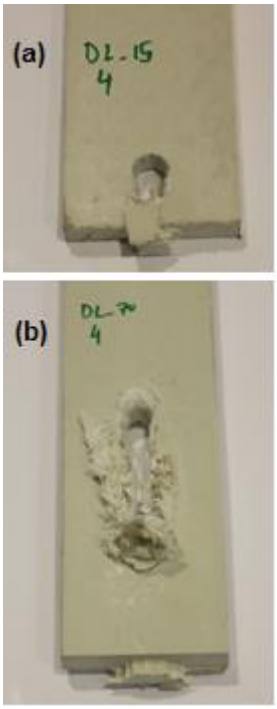

Figure 4 - Failure modes: (a) shear-out; (b) bearing.

3.4. Beam-to-column tests

Finally, four full-scale beam-to-column connection typologies (BC-3-W-M, BC-3-F-M, BC-8-F-M, BC-8-F2-M) were monotonically (M) tested. Beams and columns were cut from I-section profiles in lengths of 900 mm. Stainless steel (AISI 304) web and flange cleats were used, as well as stainless steel bolts (A2-70) with a diameter of 8 mm. Web and flange-cleated connections, W and F, respectively, were tested, varying the number of bolts and the thickness of the cleat (3 mm and 8 mm). Two specimens per batch were tested.

The web-cleated typology (BC-3-W-M) used a 30x3 mm^2 cleat with three bolts in the web of the beam and six bolts in the web of the column. As for the flange-cleated typologies, BC-3-F-M and BC-8-F-M used a 50 mm width cleat with four bolts (two in the beam and two in the column). BC-8-F2-M used a 100x8 mm^2 cleat with four bolts in the beam and four bolts in the column.

3.4.1.Setup, instrumentation and procedure

The monotonic tests were performed at *Laboratório de Estruturas e Resistência de Materiais* (LERM), at IST, using a closed steel frame. The boundary conditions of the column (clamped ends) were assured by a set of steel blocks and two steel pieces. The out-of-plane displacements of the free end of the beam were restricted by two aluminium bars. The load was applied at a distance of 580 mm from the column facing flange by a pinned loading fixture connected to a hydraulic jack with a load capacity of 250 kN and a stroke of 400 mm. A load cell (50 kN capacity) was also attached to the loading system, in series with the jack and the pins. The hydraulic jack was controlled by computer, using a software developed in *LabView*. Two rotation transducers were used to determine the rotation of the beam and column. To measure the vertical displacements of the beam one string pot displacement transducer was used. The test setup is illustrated in Figure 6.

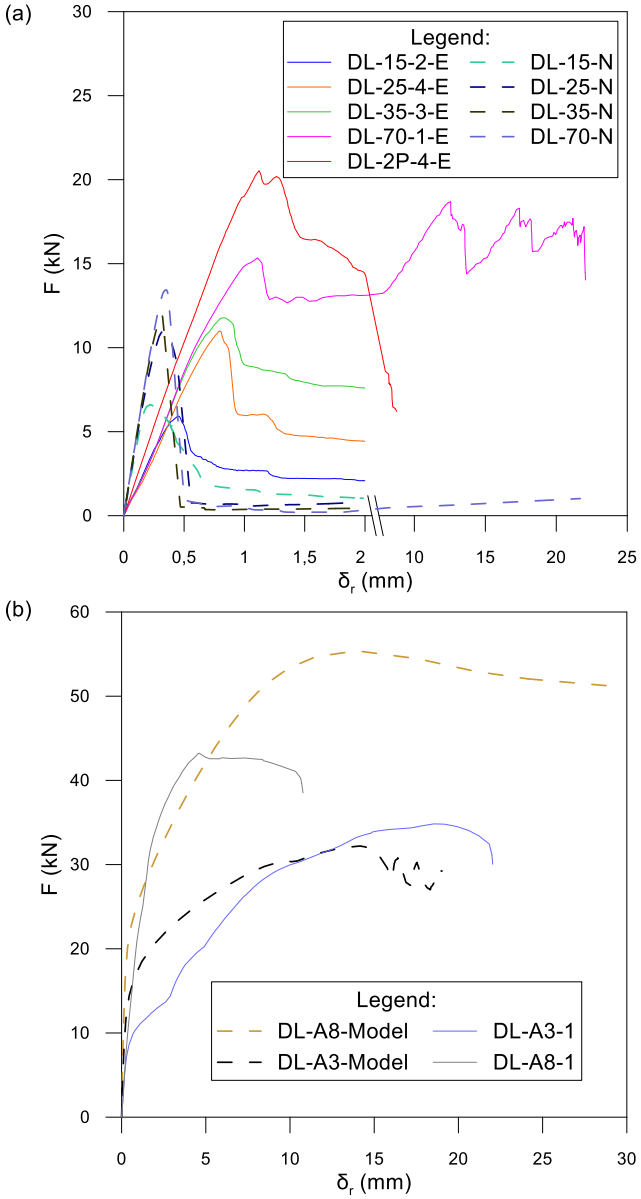

Figure 5 – Numerical and experimental double-lap connection force-displacement curves. (a) GFRP specimens; (b) stainless steel specimens.

A torque of 10 Nm was applied to the bolts. The tests were performed at a speed of 0,25 mm/s until the failure of the connection. Data was recorded at a rate of 10 Hz by a HBM, model *QuantumX* data logger.

3.4.2.Results and discussion

The experimental force-displacement curves (E) of all beam-to-column specimens are presented in Figure 7. The specimens exhibited an initial elastic behaviour until failure, which was identified by drops in the force-displacement curve.

The failure mode was due to transverse tension in the web-flange junction in every specimen tested (Figures 8 and 9); no crushing was observed on the holes. As it can be seen in Figure 10, the top cleat was deformed.

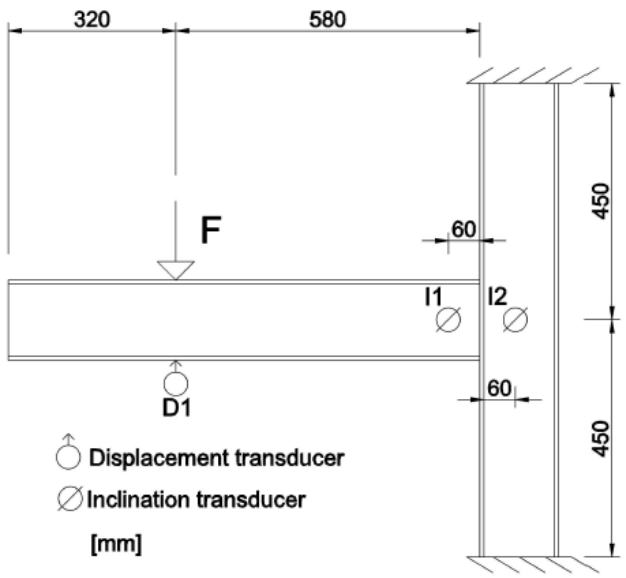

Figure 6 - Beam-to-column monotonic test setup.

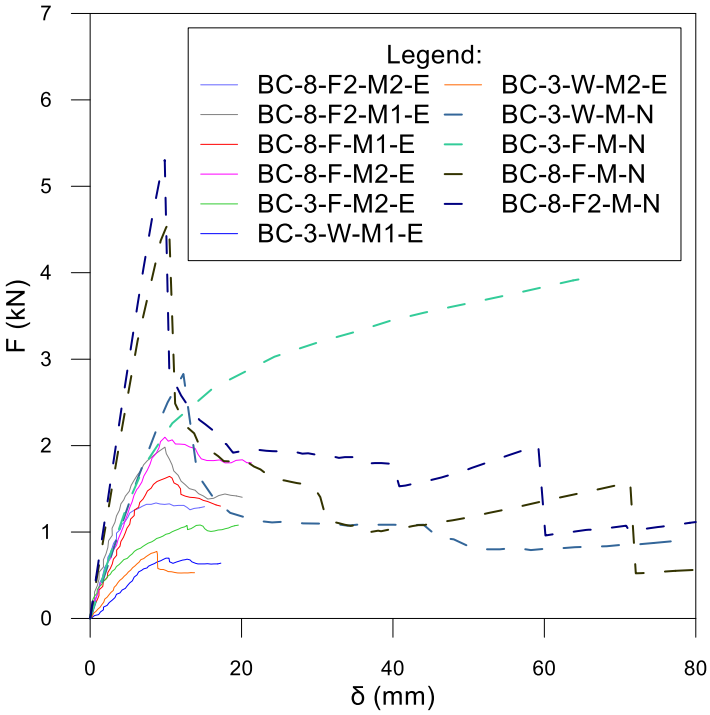

Figure 7 – Numerical and experimental beam-to-column force-displacement curves.

Figure 8 - Web-flange junction failure in column (1).

Figure 9 - Web-flange junction failure in column (2).

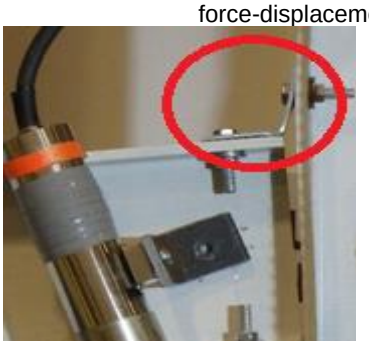

Figure 10 - Top cleat plastic deformation.

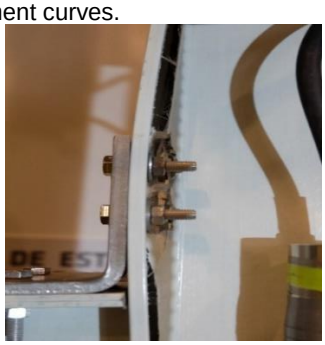

Figure 11 - Mat torn and punching shear of washer.

This substantial deformation was only observed in specimen BC-3-F-M1. In typology BC-8-F2-M the mats of the GFRP flange column were torn and there was punching shear of the washers (Figure 11).

The average results for each typology are summarized in Tables 5 and 6. In general, it was considered that the connections tested were insufficiently stiff and presented low resistance. In addition, since there was no significant drop in the force-displacement curve, there was some difficulty in the evaluation of the ductility coefficient (C_d) [35], given by (6), namely in setting the yielding (u_y) and ultimate (u_u) displacements. However, typology BC-3-F-M exhibited the highest ductility, whereas typology BC-3-W-M presented the lowest.

There was a significant difference between connections using 3 mm and 8 mm cleats. BC-8-F-M resisted to the highest loads with a small difference to BC-8-F2-M. As for stiffness (K_δ and K_θ), BC-8-F2-M registered the best performance, with values 30% to 40% higher than those of typology BC-8-F-M. This increment in stiffness may be related to the fact that the contact area between the cleat and GFRP is higher. Typology BC-3-W-M presented the lowest resistance and stiffness.

$$C_d = \frac{u_u - u_y}{u_u} \quad (6)$$

The expressions (7) and (8) allow the classification of the connection according to the rotational stiffness [36]. In the expressions (i) $S_{j,ini}$ is the stiffness; (ii) k_b is a parameter depending on the bracing system (taken as 25); (iii) $(E \times I)_b$ is the beam flexural rigidity, given by (8); and (iv) L_b is the span of the beam (taken as 2,88 m, like Martins *et al.* [37] for The Clickhouse project. In expression (9), $E_{t,L}$ is the elasticity modulus in tension in the longitudinal direction (3.2), I is the second moment of area, $A \times {d_{cg}}^2$ is the application of the Lagrange-Steiner theorem and the subscript i represents the web and the flanges.

For a rotational stiffness lower than 55,6 kNm/rad the connection is classified as pinned. On the other hand, for a rotational stiffness higher than

2779 kNm/rad the connection is classified as rigid. Considering these values, the connections using 3 mm cleats are pinned and the connections using 8 mm cleats are semi-rigid, although very close to being classified as pinned.

Table 5 - Average ultimate force, displacement and stiffness results.

Type	F_u (kN)	δ_u (mm)	K_δ (kN/m)	C_d $(-)$
BC-3-W-M	0,741	9,56	99,5	0,282
BC-3-F-M	1,08	14,6	110	0,724
BC-8-F-M	1,87	10,3	214	0,380
BC-8-F2-M	1,66	9,3	313	0,567

Table 6 - Average ultimate moment, rotation and rotational stiffness results.

Type	M_u (kNm)	$\theta_u (rad)$	K_θ (kNm/rad)
BC-3-W-M	0,43	0,016	36,4
BC-3-F-M	0,629	0,027	37,0
BC-8-F-M	1,09	0,018	68,8
BC-8-F2-M	0,964	0,017	111

$$S_{j,ini} = k_b \times \frac{(E \times I)_b}{L_b} \quad (7)$$

$$S_{j,ini} = 0{,}5 \times \frac{(E \times I)_b}{L_b} \quad (8)$$

$$(E \times I)_b = \sum_i \left(E_{t,L} \times I\right)_i + \sum_i \left(E_{t,L} \times A \times {d_{cg}}^2\right)_i \quad (9)$$

4. Numerical study

4.1. Model description

4.1.1. Geometry, mesh and discretization

All the double-lap and beam-to-column typologies tested were modelled. GFRP was modelled using continuum shell elements (SC8R) using Simpson's integration rule with three integration points. Stainless steel parts were modelled as (i) C3D8 elements for the double-lap specimens, bolts, nuts and washers; and (ii) C3D4 elements for the cleats.

Aiming to reduce computational costs, the bolt, the nut and the washer were considered a single piece. A symmetry simplification of the beam-to-column connection was made. No torque and no gap were considered for the bolts.

4.1.2. Boundary conditions

In the double-lap models, the steel end was clamped and a displacement was applied to the opposite edge. In the beam-to-column models the column edges were clamped and the out-of-plane displacements were restrained. Symmetry boundary conditions were considered and the load was applied by an imposed displacement at a distance of 580 mm from the column facing flange.

4.1.3. Contact and friction simulation

A tie restraint was applied between the web and the flanges. A frictionless hard contact was considered for the GFRP-GFRP, GFRP-nut, GFRP-cleat and cleat-nut surfaces. For surfaces in contact with the shank/thread of the bolt a frictionless hard contact and a tangential behaviour (penalty - 0,2) were defined. For the double-lap models, no contact was defined for the GFRP-steel surface.

4.1.4. Type of analysis

Hashin's damage criterion and a continuous degradation model were defined. The fracture energies consider a set of four different types of damage: (i) matrix compression; (ii) matrix tension; (iii) fiber compression; and (iv) fiber tension, presented in Table 7, adapted from El-Hajjar and Haj-Ali [38].

4.2. Double-lap models

4.2.1. Material properties

The longitudinal direction of the plates was defined as direction 1. Since GFRP is an orthotropic material, direction 2 represents both transverse directions. The elastic properties and the material's resistance (f) for the different loads (compression - C; tension - T; and shear - S) are presented in Tables 8 and 9. The 40 mm plate properties (3.2) were used.

Table 7 - Fracture energies for different types of damage [38].

$G_{f,T}$ (N/mm)	$G_{f,C}$ (N/mm)	$G_{m,T}$ (N/mm)	$G_{m,C}$ (N/mm)
23,7	23,7	8,9	8,9

Table 8 – Plate's elastic properties.

E_{11} (GPa)	E_{22} (GPa)	ν_{12} $(-)$	G_{12} (GPa)	G_{13} (GPa)	G_{23} (GPa)
32,1	3,68	0,28	2,65	2,40	2,40

Table 9 – Plate's resistant properties.

$f_{1,T}$ (MPa)	$f_{1,C}$ (MPa)	$f_{2,T}$ (MPa)	$f_{2,C}$ (MPa)	$f_{1,S}$ (MPa)	$f_{2,S}$ (MPa)
367	318	29,0	53,3	32,4	27,1

As for stainless steel, since the material experimental data were considered invalid, the material's constitutive law was determined according to Rasmussen [39] (expression (10)), where (i) $\varepsilon_{0,2}$ and $\sigma_{0,2}$ are the proof strain and stress; (ii) $E_{0,2}$ is the slope of the tangent to $(\varepsilon_{0,2}; \sigma_{0,2})$; (iii) m and n are experimental parameters (and were considered 2,7 and 5,33, respectively); and (v) ε_u is the ultimate strain. In addition, the true stress-true strain [40] effect was taken into account, according to the expressions (11) and (12), where (i) ε_{TS} and σ_{TS} are the true strain and stress, respectively; and (ii) ε_E and σ_E are the

engineering strain and stress, respectively. Thus, an elasto-plastic behaviour with an elasticity modulus of 195 GPa and a Poisson ratio of 0,30 were defined. The plastic properties for the stainless steel specimen are presented in Table 10.

$$\varepsilon = \begin{cases} \frac{\sigma}{E} + 0{,}002\left(\frac{\sigma}{\sigma_{0,2}}\right)^{n}, \sigma \leq \sigma_{0,2} \\ \frac{\sigma - \sigma_{0,2}}{E_{0,2}} + \varepsilon_u\left(\frac{\sigma - \sigma_{0,2}}{\sigma_u - \sigma_{0,2}}\right)^{m} + \varepsilon_{0,2}, \sigma > \sigma_{0,2}, \end{cases} \quad (10)$$

$$\varepsilon_{TS} = \ln(\varepsilon_E + 1) \quad (11)$$

$$\sigma_{TS} = \sigma_E \times e^{\varepsilon_{TS}} \quad (12)$$

4.2.2.Results and discussion

The numerical force-displacement curves (N) of the double-lap connections are presented in Figure 5. There was a linear elastic behaviour until failure in all GFRP models. Even though in the experiments there was crushing of the GFRP in typologies DL-70, DL-2P and DL-35 (in a smaller scale), that phenomenon could not be simulated, since all failure modes were by shear-out in a brittle manner (Figure 12).

Table 10 - Plastic properties of stainless steel specimen.

$\sigma_y\ (MPa)$	$\varepsilon_y \times 10^{-5}(m/m)$	$\sigma_u\ (MPa)$	$\varepsilon_u\ (m/m)$
190	4,74	1058	0,51

Although the stainless steel specimens' models simulated the elastic and the plastic behaviours, the stiffness was also grater than the experimental one. The failure modes involved the bearing of the specimen (Figure 13) and the failure of the bolt (Figure 14), for typologies DL-A3 and DL-A8, respectively.

The connections' stiffness was simulated with considerable imprecision. In fact, in average it was 135% greater than the experimental results. This problem had already been felt in recent works develop at IST [41, 42]. This difference might be caused by eventual gaps in the test setup. There is a high level of uncertainty about the reason why there is such a stiffness increase, which confirms the complexity of finite elements modelling. Despite this, the ultimate force was reasonably well predicted. Tables 11 and 12 present the numerical results for the double-lap connections.

Table 11 – GFRP double-lap numerical results.

Typology	DL-15	DL-25	DL-35	DL-70	DL-2P
$F_u\ (kN)$	6,61	10,9	11,9	13,4	22,7
$\delta_u\ (mm)$	0,218	0,313	0,318	0,355	0,478
$K_\delta\ (kN/m)$	37522	41570	42580	35401	52121

Table 12 - Stainless steel double-lap numerical results.

Typology	DL-A3	DL-A8
$F_u\ (kN)$	32,2	55,4
$\delta_u\ (mm)$	14,2	14,0
$K_\delta\ (kN/m)$	62577	56306

Unlike the experimental results, typology DL-2P presented a strength considerably greater than typology DL-70. In addition, the stiffness of typology DL-A3 was greater than that of typology DL-A8. In fact, the ultimate displacement was slightly identical in the models, whereas in the experimental tests there was a considerable difference.

As expected, stainless steel specimens' performance was significantly better than that of GFRP specimens. Besides, the difference between the GFRP and stainless steel specimens was more relevant in the numerical models than in the experimental campaign. Though, the potential of using stainless steel cleats is evident, since their behaviour is better than that of GFRP.

4.3. Beam-to-column models

4.3.1.Material properties

The assumptions made for defining the web (W) and flange (F) properties were as described in 4.2.1, those properties being presented in Tables 13 and 14.

Table 13 – Profile's elastic properties.

	E_{11} (GPa)	E_{22} (GPa)	ν_{12} $(-)$	G_{12} (GPa)	G_{13} (GPa)	G_{23} (GPa)
F	41,3	5,74	0,29	3,14	2,40	2,40
W	43,6	5,74	0,22	3,12	4,36	4,36

Table 14 – Profile's resistant properties.

	$f_{1,T}$ (MPa)	$f_{1,C}$ (MPa)	$f_{2,T}$ (MPa)	$f_{2,C}$ (MPa)	$f_{1,S}$ (MPa)	$f_{2,S}$ (MPa)
F	347	328	29,0	46,7	47,1	27,1
W	384	375	29,0	42,3	47,7	30,5

The normal part of the cleat was defined as in 4.2.1. The fact that the cleats were cold formed, also increased the resistance in the bent zone [43]. The constitutive law was given by (10), based on (13), where (i) r_i and t are the internal radius of the cleat and its thickness, respectively; (ii) c and a are empirical coefficients (assumed 1,881 and 0,194, respectively). Therefore, the plastic properties considered in the bent zone are presented in Table 15, assuming an elastic behaviour identical to the one described in 4.2.1.

$$\sigma_{0,2-B} = c\frac{\sigma_{0,2}}{\left(\frac{r_i}{t}\right)^{a}} \quad (13)$$

Table 15 - Plastic properties of the bent zone of the cleat.

$\sigma_y\ (MPa)$	$\varepsilon_y \times 10^{-5}\ (m/m)$	$\sigma_u\ (MPa)$	$\varepsilon_u\ (m/m)$
590	12,4	1484	0,505

4.3.2.Results and discussion

The numerical force-displacement curves (N) of the beam-to-column connections are presented in Figure 7. All typologies exhibited a linear elastic behaviour until failure, which was caused by

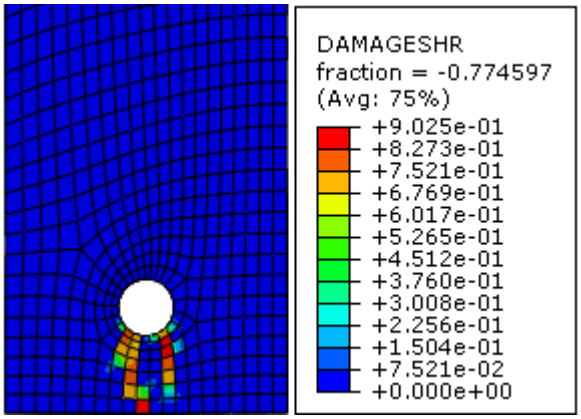

Figure 12 - Shear-out failure mode of a GFRP specimen.

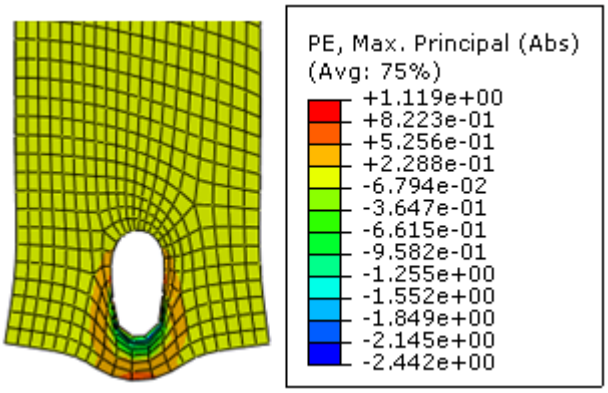

Figure 13 - Bearing capacity of a stainless steel specimen.

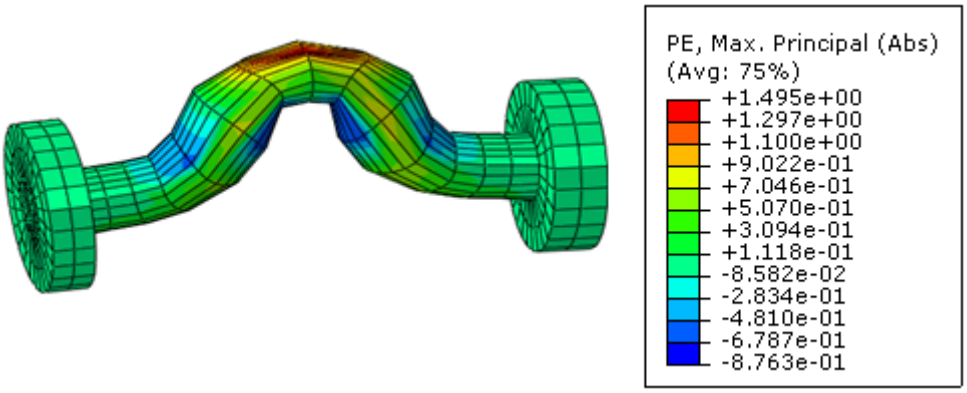

Figure 14 - Bolt failure mode (DL-A8).

transversal tension in the web-flange junction (Figure 15). The failure mode is characterized by a load drop in the force-displacement curve. Considerable stress concentrations were found in the bolts (Figure 16) and there was plastic strain in the BC-3-F-M top cleat (Figure 17), as in the experiments.

The numerical results are presented in Table 16. The connections' stiffness and strength could not be simulated with accuracy. Since the beam-to-column connections failed by transversal tension in the web-flange junction, its (local) resistance (not determined) was essential to model the connection behaviour.

There was a significant difference in strength and stiffness between typologies using 3 mm and 8 mm thick cleats. In fact, BC-8-F2-M exhibited the highest resistance and stiffness. On the other hand, the web-cleated typology resisted to the lowest loads and revealed the lowest stiffness. According to the results, there was no considerable increase of strength and stiffness by using more bolts (as in the tests). In fact, what influences the connections' performance the most is the cleats' thickness.

5. Conclusions and future developments

5.1. Conclusions

The experimental campaign developed in this dissertation started with the mechanical characterization of GFRP and stainless steel. The orthotropic behaviour of GFRP was confirmed; some anomalous results were obtained for stainless steel elasticity modulus and these were attributed to the lack of precision of the video-extensometer used.

Table 16 – Beam-to-column numerical results.

Tytopology	$F_u\ (kN)$	$\delta_u\ (mm)$	$K_\delta\ (kN/m)$
BC-3-W-M	2,83	12,3	257
BC-3-F-M	3,92	64,5	247
BC-8-F-M	4,58	10,4	522
BC-8-F2-M	5,30	9,84	586

The double-lap tests allowed to conclude that by increasing the number of bolts, the increment of strength and stiffness is insignificant. However, by varying the edge distance the failure mode is influenced. Despite this, the stiffness did not increase linearly with the increase of edge distance. In fact, there might be a plateau after which it remains approximately constant.

The inexistence of continuity mats from the web to the flanges of the GFRP profiles limited the connections performance, which resulted in web-flange failure modes. Despite this, there was a significant difference in the behaviour of typologies using 3 mm and 8 mm thick cleats. In fact, typologies BC-3-W-M and BC-3-F-M were classified as pinned. On the other hand, increasing the number of bolts may have advantages, since BC-8-F2-M exhibited the highest strength and stiffness.

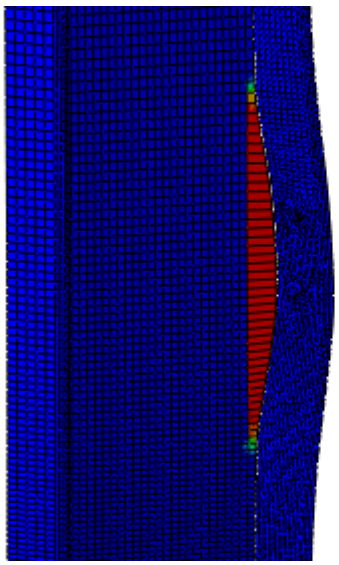

Figure 15 - Web-flange junction failure mode.

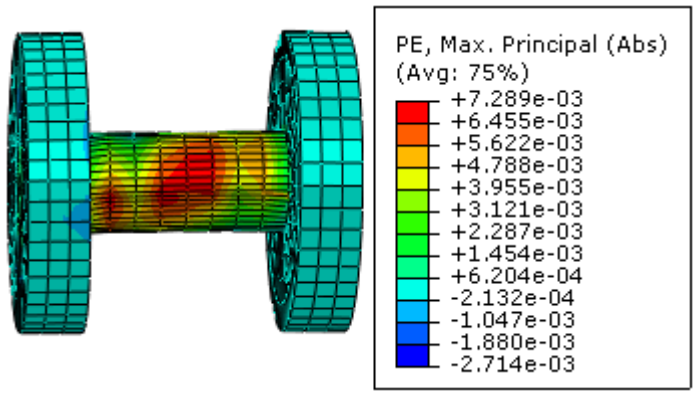

Figure 16 - Bolt concentration stress.

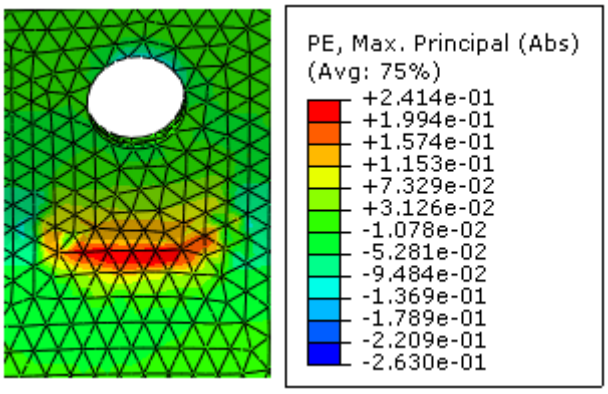

Figure 17 - Cleat plastic strain.

The stiffness of the connections modelled could not be simulated with accuracy, which had already been reported in other studies. The difference between the numerical and experimental stiffness may be related to gaps in the double-lap test setup. Despite the difference in stiffness, strength was reasonably well predicted. As for failure modes, only the shear-out mode was simulated. This suggests the need to deepen the fracture energy of the material. In beam-to-column connections, a different problem arose, related to the transverse tensile strength of GFRP, since the geometry of the profile did not allow to characterize this property. This led to over-estimated strength connections.

5.2. Future developments

The extensive study presented herein justify suggesting the following developments:

(i) Study of continuity joints by introducing a three-dimensional problem. This will allow to study the tri-dimensional behaviour of a joint or a frame.

(ii) The beam-to-column connections tested were weak and had low stiffness. Therefore, reinforcing the connections may increase their performance. The reinforcement could include threaded rods connecting both column flanges or the introduction of cleats (bonded or bolted) in the web-flange junction. Even the fiber architecture could be changed with the introduction of mats in the web-flange junction.

(iii) Cyclic tests were not performed, since the connections were weak and presented low stiffness. This kind of tests would allow the characterization of the seismic behaviour of the connections (or the frame).

(iv) All the above mentioned issues can be assessed not only experimentally but also by developing numerical finite element models.

(v) One of the main obstacles for the development of the numerical models was (apparently) the inaccurate fracture energy values used. A further study of these parameters could lead to more realistic models.

6. References

[1] J. R. Correia, “Compósitos de Matriz Polimérica”, in Ciência e Engenharia de Materiais de Construção, 1st ed., IST Press, 2012, pp. 573–636.

[2] J. T. Mottram, “Design Guidance for Bolted Connections in Structures of Pultruded Shapes: Gaps in Knowledge”, in Seventeenth Int. Conf. Composite Materials, 2009.

[3] J. T. Mottram and G. J. Turvey, “Physical test data for the appraisal of design procedures for bolted joints in pultruded FRP structural shapes and systems”, Prog. Struct. Eng. Mater., vol. 5, no. 4, pp. 195–222, 2003.

[4] C. Cooper and G. J. Turvey, “Effects of joint geometry and bolt torque on the structural performance of single bolt tension joints in pultruded GRP sheet material”, Compos. Struct., vol. 32, no. 1–4, pp. 217–226, 1995.

[5] A. M. Girão Coelho and J. T. Mottram, “A review of the behaviour and analysis of bolted connections and joints in pultruded fibre reinforced polymers”, Mater. Des., vol. 74, pp. 86–107, 2015.

[6] L. C. Bank, Composites for Construction: Structural Design with FRP Materials. Hoboken, New Jersey: John Wiley & Sons, Inc., 2007.

[7] Y. Xiao and T. Ishikawa, “Bearing strength and failure behavior of bolted composite joints. Part I: Experimental investigation”, Compos. Sci. Technol., vol. 65, no. 7–8, pp. 1022–1031, 2005.

[8] Y. Xiao and T. Ishikawa, “Bearing strength and failure behavior of bolted composite joints. Part II: Modelling and simulation”, Compos. Sci. Technol., vol. 65, no. 7–8, pp. 1022–1031, 2005.

[9] F. Ascione, L. Feo and F. Maceri, “An experimental investigation on the bearing failure load of glass fibre/epoxy laminates”, Compos. Part B Eng., vol. 40, no. 3, pp. 197-205, 2008.

[10] S. Abd-El-Naby and L. Hollaway, “The experimental behaviour of bolted joints in pultruded glass/polyester material. Part 2: Two-bolt joints”, Composites, vol. 24, no. 7, pp 531–538, 1993.

[11] S. Abd-El-Naby and L. Hollaway, “The experimental behaviour of bolted joints in pultruded glass/polyester material. Part 1: Single-bolt joints”, Composites, vol. 24, no. 7, pp. 531–538, 1993.

[12] N. K. Hassan, M. A. Mohamedien and S. H. Rizkalla, “Multibolted Joints FOR GFRP Structural Members”, J. Compos. Constr., vol 1, no. 1, pp. 3–9, 1997.

[13] J. Clarke, Strutcutral Design of Polymer Composites - EUROCOMP Design Code and handbook. London, UK: E & FN Spon, 1996.

[14] Italian National Research Council, Guide for the Design and Construction of Fiber-Reinforced Concrete Structures. Rome, 2007.

[15] Joint Research Centre, Prospect for New Guidance in the design of FRP. Brussels, 2016.

[16] L. C. Bank, A. S. Mosallam and H. E. Gonsior, “Beam-to-column connections for pultruded FRP shapes”, Serv. Durab. Constr. Mater., pp 804–813, 1990.

[17] L. C. Bank, A. S. Mosallam and G. T. McCoy, “Design and Performance of Connections for Pultruded Frame Structures”, J. Reinf. Plast. Compos., vol. 13, no. 3, pp. 199–212, 1994.

[18] A. S. Mosallam, M. K. Abdelhamid and J. H. Conway, “Performance of Pultruded FRP Connections under Static and Dynamic Loads”, J. Reinf. Plast. Compos., vol. 13, no. 5, pp. 386-407, 1994.

[19] L. Bank, J. Yin, L. Moore, D. Evans and R. Allison, “Experimental and Numerical Evaluation of Beam-To-Column Connections for Pultruded Structures”, J. Reinf. Plast. Compos., vol. 15, no. 101052–1067, 1996.

[20] S. Smith, I. D. Parsons and K. D. Hjelmstad, “Experimental Comparisons of Connections for GFRP Pultruded Frames”, J. Compos. Constr., vol. 3, pp. 20–26, 1999.

[21] J. Qureshi and J. Toby Mottram, “Moment-rotation response of nominally pinned beam-to-column joints for frames of pultruded fibre reinforced polymer”, Constr. Build. Mater., vol. 77, pp. 396–403, 2015.

[22] J. Qureshi and J. T. Mottram (2012), “Moment-Rotation Behaviour of Beam-To-Column Joints For Simple Frames of Pultruded Shapes”, in 6th Int. Conf. on FRP Composites in Civil Engineering - CICE 2012.

[23] J. Qureshi and J. T. Mottram, “Response of Beam-To-Column Web Cleated Joints For FRP Pultruded Members”, J. Compos. Constr., vol 18, no. 2, pp. 1–11, 2013.

[24] J. Qureshi and J. T. Mottram, “Behaviour of pultruded beam-to-column joints using steel web cleats", Thin-Walled Struct., vol. 73, pp 48–56, 2013.

[25] C. Hühne, A. K. Zerbst, G. Kuhlmann, C. Steenbock and R. Rolfes, “Progressive damage analysis of composite bolted joints with liquid shim layers using constant and continuous degradation models”, Compos. Struct., vol. 92, no. 2, pp. 189–200, 2010.

[26] C. T. McCarthy, M. A. McCarthy and V. P. Lawlor, “Progressive damage analysis of multi-bolt composite joints with variable bolt-hole clearances”, Compos. Part B Eng., vol. 36, no. 4, pp. 290–305, 2005.

[27] C. T. McCarthy, M. A. McCarthy, W. F. Stanley and V. P. Lawlor, “Experiences with Modeling Friction in Composite Bolted Joints”, J. Compos. Mater., vol. 39, no. 21, pp. 1881-1908, 2005.

[28] C. T. McCarthy and M. A. McCarthy,

"Three-dimensional finite element analysis of single-bolt, single-lap composite bolted joints: Part I - model development and validation", Compos. Struct., vol. 71, no. 2, pp. 140–158, 2005.

[29] C. T. McCarthy and M. A. McCarthy, "Three-dimensional finite element analysis of single-bolt, single-lap composite bolted joints: Part II - Effects of bolt-hole clearance", Compos. Struct., vol. 71, no. 2, pp. 159–175, 2005.

[30] C. Casalegno, A. Picariello and S. Russo, "Analysis of all-GFRP beam-column bolted joints through progressive failure approach", Compos. Struct., vol. 33, no. 2, pp. 81–87, 2012.

[31] C. Casalegno and S Russo, "Structural joints made by FRP and steel: A new proposal of analysis based on the progressive damage approach", Compos. Mech. Comput. Appl., vol. 6, no. 2, pp. 1–18, 2015.

[32] J. Gonilha, "Concrete hybrid structural systems. Application to the development of a footbridge prototype", PhD thesis in Civil Engineering, Instituto Superior Técnico, University of Lisbon, 2014.

[33] American Composites Manufacturers Association, Pre-Standard for Load & Resistance Factor Design (LRFD) of Pultruded Fiber Reinforced Polymer (FRP) Structures. 2010.

[34] CEN. EN 1993-1-4. Eurocode 3 - Design of steel structures - Part1.4, European Committee for Standardization, Brussels, 2010.

[35] A. Jorissen and M. Fragiacomo, "General notes on ductility in timber structures", Eng. Struct., vol. 33, no. 11, pp. 2987–2997, 2011.

[36] CEN. EN1993-1-8. Eurocode 3 - Design of steel structures - Part 1-8, European Committee for Standardization, Brussels, 2010.

[37] D. Martins, M. Proença, J. R. Correia, J. Gonilha, M. Arruda and N. Silvestre, "Development of a novel beam-to-column connection system for pultruded GFRP tubular profiles" (In preparation), 2017.

[38] R. El-Hajjar and R. Haj-Ali, "Mode-I fracture toughness testing of thick section FRP composites using the ESE(T) specimen", Eng. Fract. Mech., vol. 72, no. 4, pp. 631–643, 2005.

[39] K. J. Rasmussen, "Full-range Stress-strain Curves for Stainless Steel Alloys", Univ. Sydney, Sydney NSW Res. Rep. No R811, 2001.

[40] Y. Ling, "Uniaxial True Stress-Strain after Necking", AMP J. Technol., vol. 5, no. 1, pp. 37–48, 2004.

[41] M. Proença, "Comportamento de ligações aparafusadas entre perfis de compósito GFRP", MSc dissertation in Civil Engineering, Instituto Superior Técnico, 2015.

[42] J. Azevedo, "Desenvolvimento de um sistema inovador para ligações entre perfis de compósito de GFRP", MSc dissertation in Civil Engineering, 2016.

[43] P. A. Sloof and R. M. Schuster (2000), "Yield Strength Increase of Cold Formed Sections Due to Cold Work of Forming", in 15th Int. Spec. Conf. on Cold-Formed Steel Structures.